Available online at www.sciencedirect.com
ScienceDirect
Ceramics International 38 (2012) 357–365
CERAMICS INTERNATIONAL
www.elsevier.com/locate/ceramint

Water-based tape-casting of SOFC composite 3YSZ/8YSZ electrolytes and ionic conductivity of their pellets

Crina Suciu [a], Hanna Tikkanen [a,b,*], Ivar Wærnhus [a], Firuta Goga [c], Eugen Dorolti [d]

[a] Prototech AS, Fantoftveien 38, NO-5075 Bergen, Norway
[b] University of Bergen, Institution of Physics and Technology, Allégaten 55, NO-5007 Bergen, Norway
[c] Babes-Bolyai University, Faculty of Chemistry and Chemical Engineering, Arany Janos 1, 400028 Cluj-Napoca, Romania
[d] Babes-Bolyai University, Faculty of Physics, 400084 Cluj-Napoca, Romania

Received 21 June 2011; received in revised form 5 July 2011; accepted 5 July 2011
Available online 18th July 2011

Abstract: Electrolyte supports for SOFC applications were obtained by water-based tape-casting. Slurries of commercial 3YSZ and 8YSZ and mixtures with a mass ratio of 25/75 and 75/25, respectively, were prepared. A commercial acrylic polymer binder with dispersive properties was used. The drying conditions for obtaining crack-free green tapes were studied. Crack formation during drying was greatly affected by the carrier speed at a fixed temperature. Thermal analysis was performed on the green tapes to study the binder burn out properties. Weight loss of the green tapes occurred until 400 °C and a pre-heating step was therefore included in the sintering program. The microstructure of the green and sintered tapes were investigated by SEM. Fully densified tapes were obtained after sintering at 1450 °C. The ionic conductivity of pressed pellets were characterized by impedance spectroscopy in the temperature range of 200–1000 °C. Phase and crystal structure of pressed pellets were analyzed by XRD. The crystallinity varied from a majority of monoclinic structure (pure 3YSZ) to a majority of tetragonal structure with increasing the 8YSZ content. A cubic single phase structure was obtained by further increasing the 8YSZ content. It was shown that the ionic conductivity of the composite samples were modified with respect to the pure materials. At high temperatures the pure cubic structure gave rise to high conductivity. At low temperatures the conductivity was affected by the grain boundary resistance which was the lowest for the pure 3YSZ, the highest for the pure 8YSZ and decreased as a function of increasing 8YSZ content.

Keywords: C. Impedance; Water-based tape-casting; Yttria-stabilized zirconia; Composite materials; Solid oxide fuel cell

1. Introduction

Solid oxide fuel cells (SOFCs) are electrochemical devices for producing electricity [1]. They have received a lot of attention due to their high conversion efficiency and low pollutant emissions.

In solid oxide fuel cells the electrolytes are subjected to varying physical and chemical environments during operation [1]. In addition to exhibiting resistance to these environments the electrolyte material has to possess high ionic conductivity and low electronic conductivity at the operating temperatures of SOFCs. In the planar SOFC configuration the supporting structure is either one of the electrodes or the electrolyte. Since the cell resistance is dependent on the electrolyte thickness the electrolyte should be as thin as possible.

Yttria doped zirconia (YSZ) is the most frequently used material in SOFC electrolytes. Zirconia doped with 8 mol% of yttria (8YSZ) with the cubic crystal structure has the highest ionic conductivity [2,3]. Unfortunately, the mechanical properties of 8YSZ are poor preventing its use in the electrolyte-supported SOFC configuration [4]. In contrast, the tetragonal structure associated with low dopant concentrations, such as 3 mol% of yttria, exhibits good mechanical properties [2,5–7]. This explains the wide use of 3YSZ as raw material for self-supported electrolyte SOFC configuration despite its lower ionic conductivity [2,3].

In a recent study by Ghatee et al. the effects of mixing 3YSZ with 8YSZ on the electrical and mechanical properties of the resulting samples were investigated [8]. The results suggest that addition of 3YSZ to pure 8YSZ improves the fracture toughness and strength of the resulting composite materials.

* Corresponding author at: Prototech AS, Fantoftveien 38, NO-5075 Bergen, Norway. Tel.: +47 94 14 03 46; fax: +47 56 57 41 14.
E-mail addresses: hanna.tikkanen@prototech.no, hanna-mari.tikkanen@ift.uib.no (H. Tikkanen).

0272-8842/$36.00
doi:10.1016/j.ceramint.2011.07.014

Impedance measurements also revealed that addition of 3YSZ modifies the electrical properties with respect to the pure 8YSZ. Their results suggest that composite electrolytes can be used to design solid electrolytes with improved performance.

Tape-casting is a method for obtaining large-area thin ceramic films [9]. The tape-casting process consists of preparing a slurry containing the ceramic particles of interest and casting this slurry with the help of a doctor blade on a moving carrier material. The obtained wet cast goes through a drying chamber where the solvent is evaporated resulting in a dried green ceramic tape. Typically, organic solvents are favoured in the tape casting process due to their fast evaporation rate. However, the use of organic solvents raises some environmental and health concerns.

In recent years, water-based tape-casting for obtaining SOFC components has been reported in the literature. Water-based tape casting has been used to fabricate anodes [10,11], electrolytes [7,11–15] and interconnects [16]. The objective of this study is to fabricate composite electrolyte supports from commercial 3YSZ and 8YSZ powders by aqueous tape-casting. In order to obtain crack-free green tapes the drying conditions have been studied. The sintering of the green tapes to obtain the final product has been optimized with respect to the removal of the slip additives. In addition, the effect of mixing 3YSZ and 8YSZ on the ionic conductivity in comparison with the pure materials has been investigated.

2. Experimental

2.1. Slurry preparation

Slurries for tape casting were obtained by preparing batches with different weight ratios of the following two powders: 8YSZ (TZ-8Y, Tosoh) and 3YSZ (TZ-3Y-E, Tosoh). Batches of four types were prepared: one containing only 3YSZ, one containing only 8YSZ and two mixtures with mass ratio of 25/75 and 75/25 of 3YSZ and 8YSZ, respectively.

The slurries were prepared in two stages (see the flow chart in Fig. 1). First, the appropriate amount of powders were weighted. A commercial water solution of acrylic polymer binder (WB4101, Polymer Innovations, Inc.) was added together with deionized (DI) water. The pH of the slurry was adjusted by addition of ammonia (pH $\sim$ 8). This was done to enhance the dispersive properties of the acrylic polymer binder. To avoid foaming during milling a defoamer (WB001, Polymer Innovations, Inc.) was added. The slurries were then ball milled for 16 h. In the second stage, more binder and defoamer were added and the ball milling process was continued for 4 h. The relative amounts of the starting materials are listed in Table 1

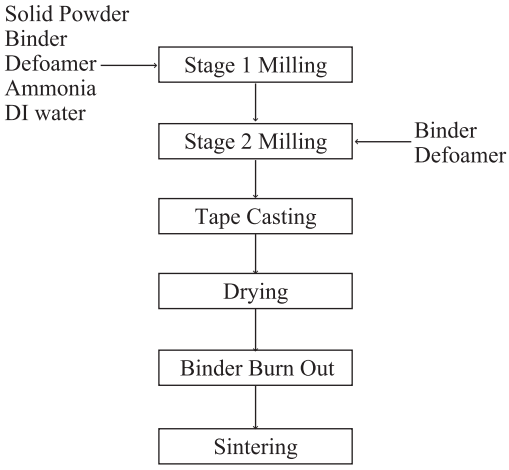

Fig. 1. Flow chart of tape preparation.

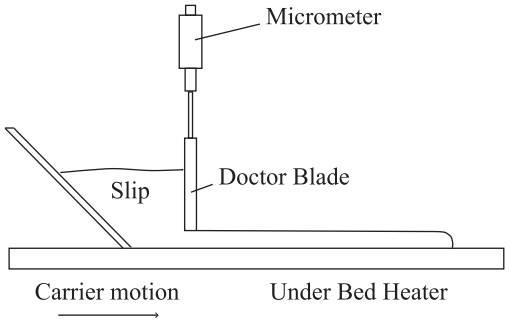

Fig. 2. Scheme of the tape casting set up.

2.2. Tape-casting

Tape-casting of the slurries were performed using a laboratory-scale tape-caster (Model NO TC-71LC, Pro-Cast, Precision Tape Casting Equipment, Division of Hed International, Inc.). Casts were obtained on a Mylar film (Richard E. Mistler, Inc.) with a casting speed v of 160–780 mm/min and a gap height of the doctor blade casting head of 0.3 and 0.28 mm. The under-bed heating temperature was set to 50 °C. A scheme of the set up is represented in Fig. 2.

The burn-out properties of the additives were studied by Thermogravimetric Analyses (TGA) and Differential Scanning Calorimetry (TG-DTA) using a Simultaneous Differential Technique Analyzer, SDT Q600 simultaneous TGA/DSC instrument (TA Instruments, USA). The green tapes were sintered according to the sintering program represented in Fig. 3. The applied sintering program had a slow heating rate of 40 °C/h until 650 °C and a final sintering temperature of 1450 °C. A Zeiss Supra 55VP Scanning Electron Microscope (SEM) was used to characterize the microstructure of the green and sintered tapes.

Table 1
Starting compounds.

	Powder (w%)	WB4101 (w%)	DF002 (w%)	DI water (w%)	NH_4OH (w%)
1. Stage	48.1	7.0	0.3	30.1	0.2
2. Stage	–	14.0	0.3	–	–

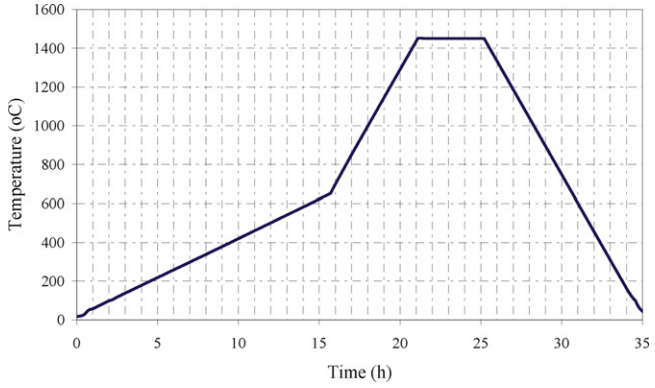

Fig. 3. Sintering scheme.

2.3. Impedance measurements

Electrical impedance spectroscopy (EIS) was used to measure the ionic conductivity of the electrolyte samples. The samples were obtained by pressing with an uniaxial press (600 bars) followed by cold isostatic pressing (CIP) at 1200 bars for 2 min. The obtained pellets were then sintered using the following sintering program: heating of 200 °C/h up to 1450 °C followed by a dwell time of 2 h and a cooling at a rate of 200 °C/h. The density of the sintered samples was measured by Archimedes method. The theoretical densities used in the calculations were 6.05 and 5.90 g/cm^3 for pure 3YSZ and pure 8YSZ, respectively [17]. The theoretical density of the composite samples can be calculated as follows:

$$\sum_{i=1}^{N} \rho_i v_i, \quad (1)$$

where ρ_i is the density of the i th powder and v_i is its volume fraction. The pressed and sintered pellets exhibited relative densities above 94% which is sufficient for impedance measurements. The surface features of the sintered electrolyte pellets were investigated by SEM.

The impedance of the electrolyte material was measured using a four-probe method; two platinum wires were used to apply the voltage over the sample and two platinum wires functioned as current collectors. The platinum wires were attached to platinum foils which functioned as electrodes. Platinum (Leitplatin 308A, Product # 64020040, Demetron) was painted on both sides of the pellet to give good electrical contact between the electrolyte sample and the platinum foil electrodes. A Solartron analytical 1260 Impedance/Gain-Phase Analyser was used to obtain the ionic conductivity. A scheme of the EIS set up is represented in Fig. 4. All the measurements were performed in the temperature range of 200–1000 °C and the data were analyzed using the ZPlot software.

2.4. X-ray measurements

X-ray diffraction analysis of the commercial sintered pellets (see Section 2.3) were performed on a Bruker D8 Advance Diffractometer using Cu K-α 1 radiation (λ = 1.540598 Å).

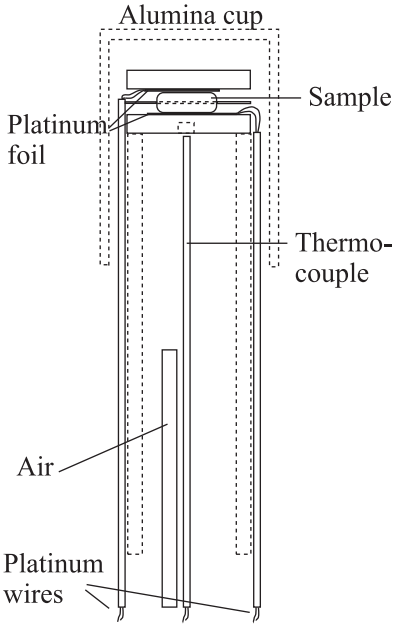

Fig. 4. Scheme of the EIS setup.

Data were collected at room temperature in the 2θ range of 20–90°. The cell parameters and the crystal structures were refined by the Rietveld method using the FullProf program code [18].

3. Results and discussion

3.1. Burn-out properties of the slip additives

The obtained green tapes consist of the ceramic particles and the slip additives. The burning of the additives should take place at lower temperatures than the sintering of the particles in order to avoid cracking of the ceramic body [19]. During thermal decomposition both gaseous and solid reaction products may be formed.

Fig. 5 shows the TG-DTA curves of the 8YSZ green film. Up to 100 °C an endothermic effect appears due to the water elimination. Between 100 and 425 °C four exothermic effects accompanied with a significant weight loss take place. These effects are due to the oxidation of the organic slip additives. The total weigh loss of the whole process is 13.83%.

The results of the thermal analysis were used to optimize the sintering program. In order to remove the slip additives in a controlled manner a slow heating rate (40 °C/h) until 650 °C was applied. The sintering of ceramic particles start approximately at 1000 °C [20]. Below this temperature the ceramic particles form a loose network permitting any gaseous species to freely diffuse.

3.2. SEM analysis of the green and the sintered tapes

It was noticed that the carrier speed was one important parameter affecting the quality of the obtained green tapes in the casting process. Carrier speed below 575 mm/min at the under-bed heating temperature of 50 °C resulted in severe cracking of the green tape. This can be due to the over drying of the tape surface. In contrast, a carrier speed above 575 mm/min

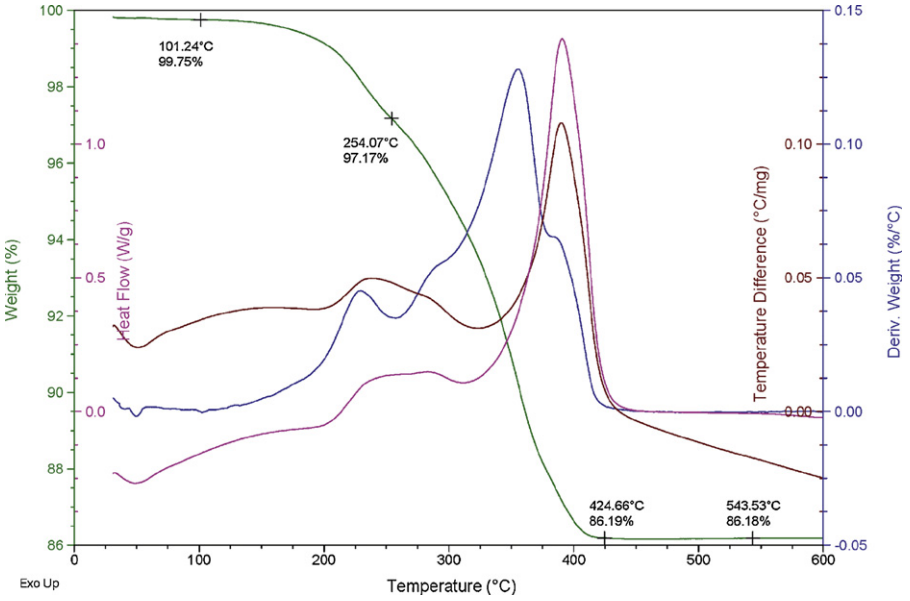

Fig. 5. Thermal analysis of the binder burn out process.

did not provide enough time for the green film to dry. By optimizing the carrier speed for the applied under-bed heating temperature crack-free and flexible green tape were obtained.

The obtained green tape thickness was approximately 120 μm. The linear shrinkage of the green tapes was studied (not shown here) by dilatometer measurements the results of which indicate that the tapes undergo a shrinkage of almost 30% during the sintering process. This was also confirmed by SEM analysis.

The microstructure of the green and sintered tapes are shown in Figs. 6 and 7, respectively. The SEM images of the green tapes (Fig. 6) exhibit some larger pores in the green structure. This is probably due to the slurries not being fully dispersed leading to a less homogeneous packing of the particles. Further work includes optimizing the slurry parameters, such as the zeta potential, viscosity and the ceramic loading, in order to achieve a more homogeneous particle packing.

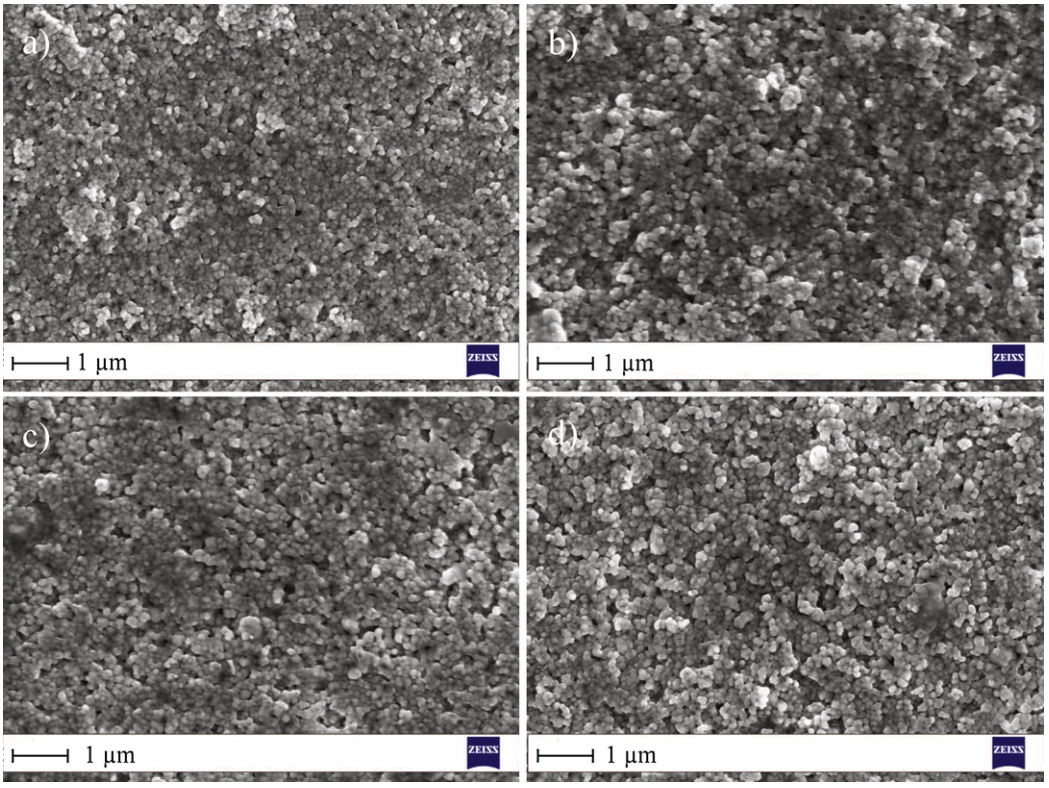

Fig. 6. SEM images of green electrolyte tapes (a) 3YSZ, (b) 3YSZ + 8YSZ 75/25, (c) 3YSZ + 8YSZ 25/75 and (d) 8YSZ.

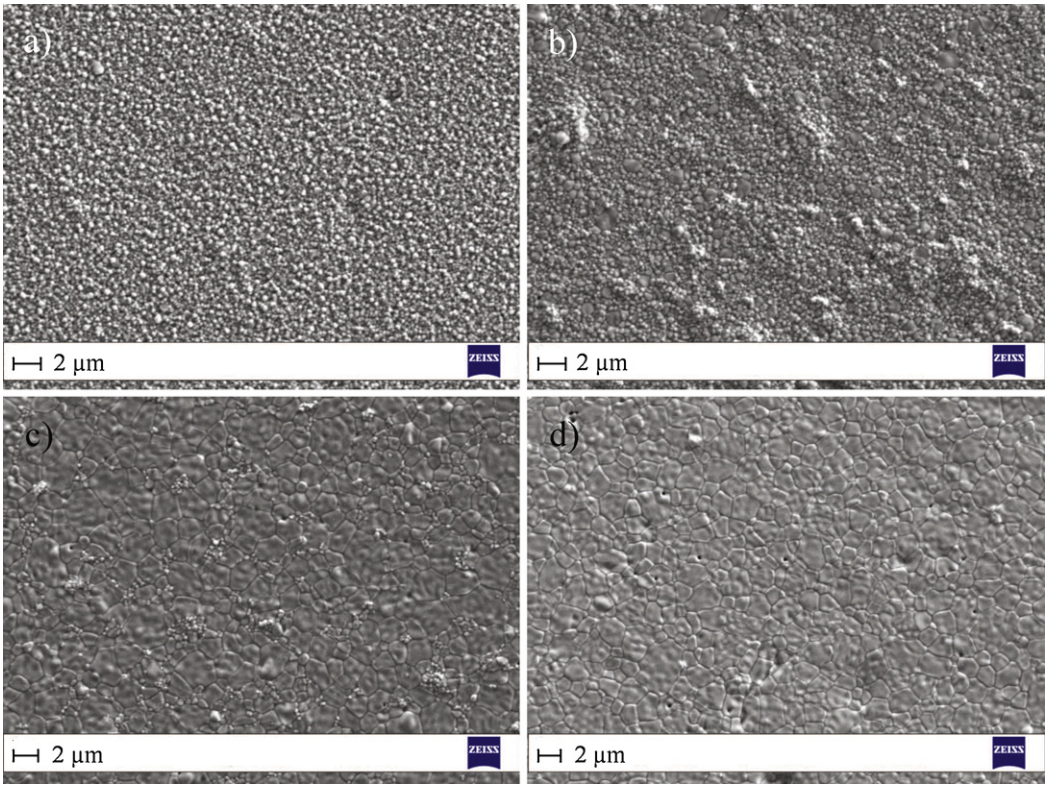

Fig. 7. SEM images of sintered electrolyte tapes (a) 3YSZ, (b) 3YSZ + 8YSZ 75/25, (c) 3YSZ + 8YSZ 25/75 and (d) 8YSZ.

The SEM images of the sintered tapes (Fig. 7) show a fully sintered microstructure. The grain size of the sintered 3YSZ is smaller than the grain size of the sintered 8YSZ. The presence of grains of two different sizes is clearly visible in the composite samples. In general, large grains can be associated with the cubic phase and small grain structure with the tetragonal phase [2].

3.3. Electrical properties

Impedance spectroscopy is a widely used tool in the study of electrical properties of solid electrolytes. The principles giving rise to the ionic conductivity in ceramic electrolytes such as doped zirconia are well known; it is due to hopping of oxide ions via vacancies in the structure [1,3]. Pure zirconia exhibits low conductivity due to the low concentration of oxide ion vacancies. As dopants with reduced valances of that of the host zirconia are added oxygen vacancies are created subsequently increasing the conductivity. The vacancy concentration is dependent on the dopant level and from a statistical viewpoint the maximum conductivity would be expected to be reached when half of the oxygen positions are vacancies. However, in practice the maximum conductivity occurs at much lower dopant concentration and in the group of YSZ materials the conductivity peaks at around a doping level of 8% (8YSZ) at high temperatures [1,3].

Fig. 8 shows an example of an impedance plot for the pure and composite samples measured at 450 °C. The measured response at this temperature resulted in three semicircles where the high-frequency response corresponds to the grain interior and the intermediate frequency response to the grain boundary conductivity. The third semicircle appearing at the low frequency end corresponds to the electrode response [21]. The measured responses were fitted to the equivalent circuit depicted in Fig. 8. The equivalent circuit consists of an inductor, L, three resistors, R and three constant phase elements, CPE. Each parallel resistor/constant phase element set corresponds to one semicircle in the complex impedance plane. The

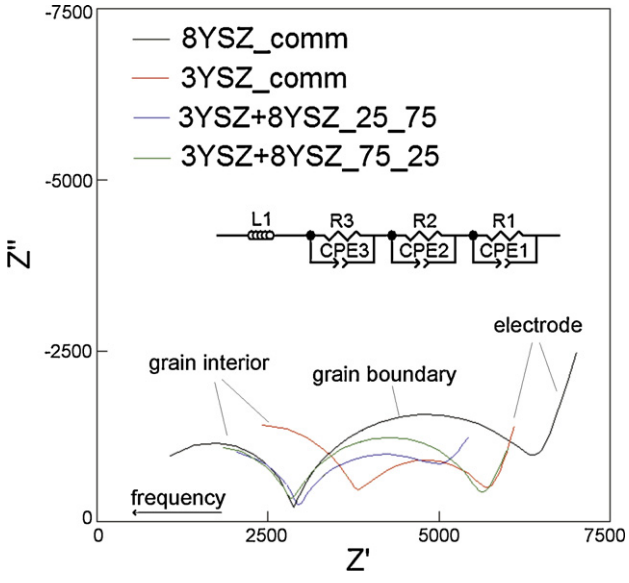

Fig. 8. Impedance measurements of the pure and composite samples.

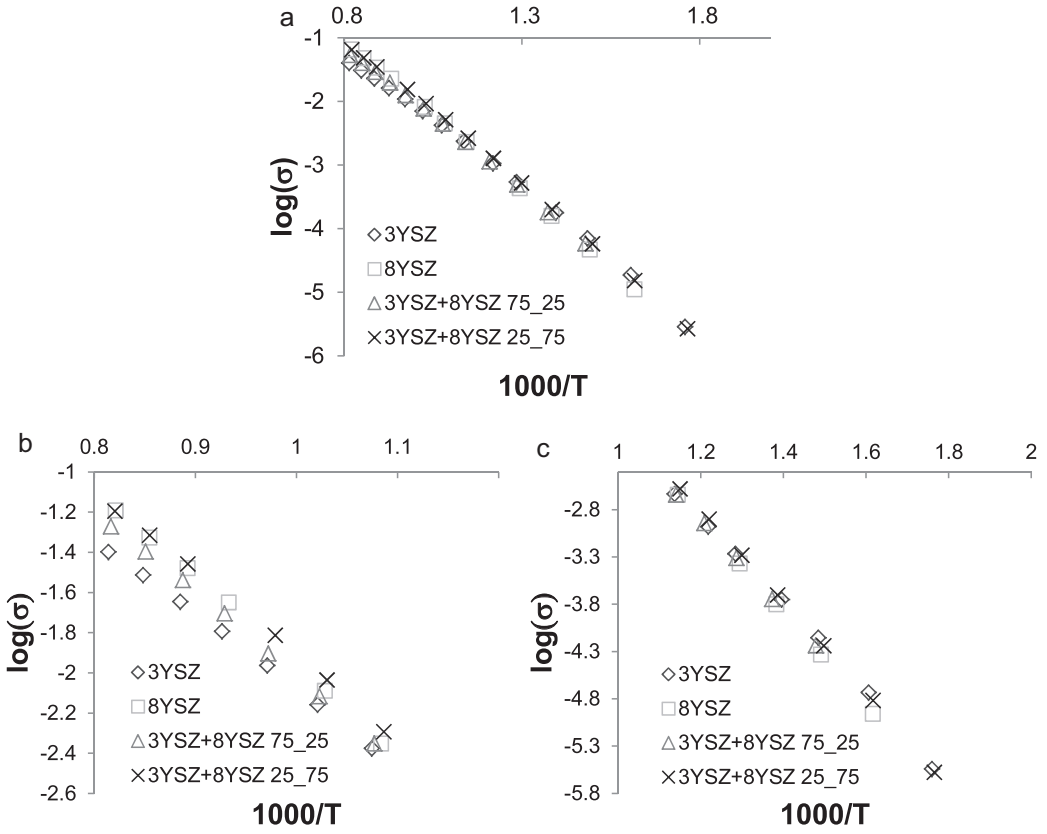

Fig. 9. Arrhenius plot of (a) the total conductivity of the pure and composite samples in the whole temperature range and a close-up of the conductivity in (b) the high temperature range and in (c) the low temperature range.

inductance, L, is a result of the inductance in the experimental setup. From the fitting a value for the radius of each semicircle corresponding to the resistivity of each contribution can be found. The values for resistivity, i.e. the reciprocal of the conductivity were used to the build the Arrhenius plots.

Fig. 9(a) shows the Arrhenius plots of the total conductivity for the pure and composite samples. At high temperatures ($\geq$650 °C, see Fig. 9(b)) the pure 3YSZ exhibits the lowest conductivity. The conductivity of the composite samples increases with increasing 8YSZ content at high temperatures. The conductivity of the composite sample with 75% of 8YSZ corresponds to that of the pure 8YSZ sample. In the low temperature regime (<650 °C, see Fig. 9(c)), the pure 3YSZ sample exhibits the highest conductivity and the pure 8YSZ the lowest. The conductivity of the composite samples decreases with increasing 3YSZ content. The observed trend in the total conductivity agrees well with the results obtained by Ghatee et al. [8] in the high temperature regime. In the low temperature regime, the conductivity of the composite samples increased with increasing 3YSZ content. It should be noted, however, that the composite systems studied by Ghatee et al. contained a maximum of 35% of 3YSZ. Also the abrupt change in the activation energy (=the slope of the Arrhenius plot) at 550 °C noted by Ghatee et al. was not observed in the present study. Instead, the slope of the Arrhenius plot decreases with increasing temperature. This decrease in the activation energy is consistently observed in various zirconia-based systems [2].

As seen in Fig. 8 the total resistivity of the material as a whole can be resolved in grain interior and grain boundary contributions. Here the grain interior resistance is the same for all the samples with 8YSZ in them but larger for the pure 3YSZ. It can be speculated if all the current goes through the 8YSZ grains at this temperature. In contrast, the grain boundary resistance is much smaller for pure 3YSZ sample and larger in the pure 8YSZ. This might explain why a mixture could perform better than the two separately.

In order to study the grain interior and grain boundary contributions over the whole temperature regime the corresponding Arrhenius plots of the conductivity for these two are represented in Fig. 10(a) and (b), respectively. The grain interior conductivities of the pure and composite samples seem to be more or less overlapping 8YSZ showing the highest conductivity. In contrast, the grain boundary conductivity exhibits a greater dependence on the material/s of which the samples are made of. Below 600 °C the measured grain boundary conductivities show a clear trend; the pure 3YSZ exhibiting the highest, the pure 8YSZ the lowest conductivity and the conductivities of the composite samples increasing with increasing 8YSZ content.

The grain boundary conductivity can be correlated with the microstructure of the samples. SEM images of polished and thermally etched electrolyte pellets after EIS measurements are represented in Fig. 11. The grain size, G, of the samples were determined by the mean linear intercept method. The mean

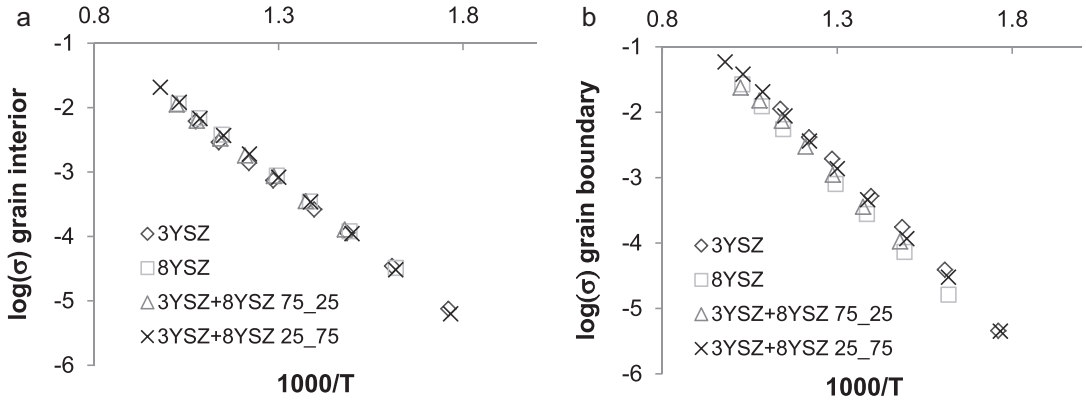

Fig. 10. Arrhenius plot of (a) the grain interior and (b) the grain boundary conductivity of the pure and composite samples.

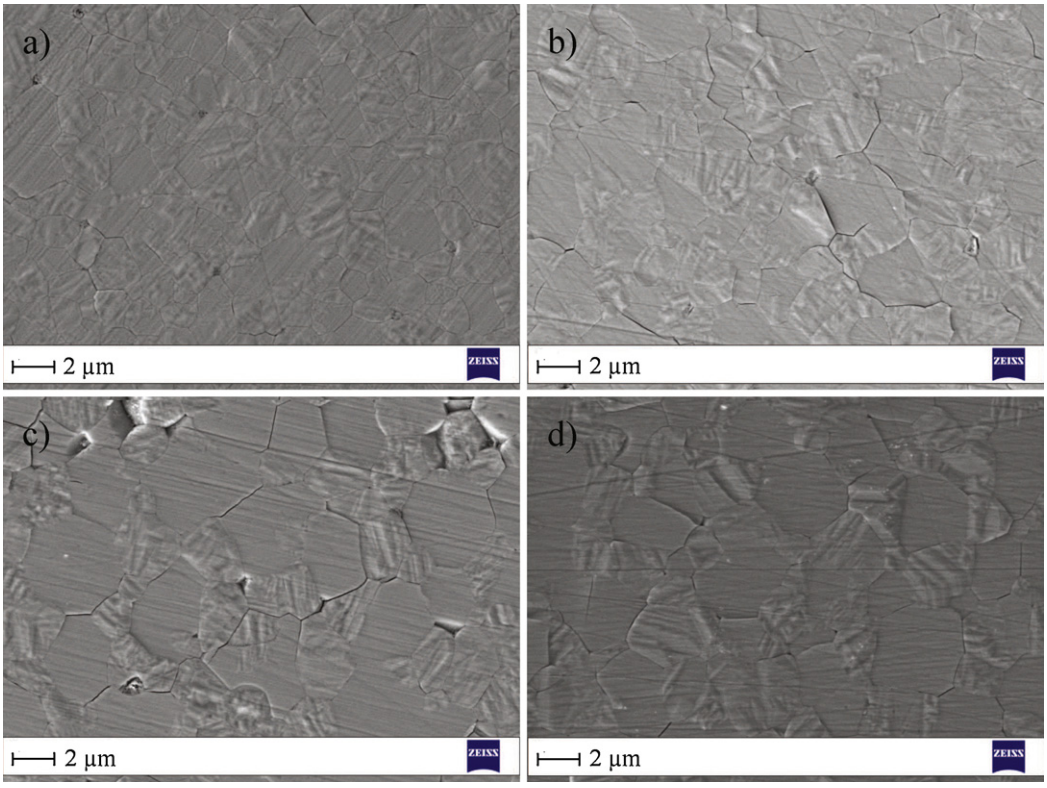

Fig. 11. SEM images of polished and thermally etched electrolyte pellets (a) 3YSZ, (b) 3YSZ + 8YSZ 75/25, (c) 3YSZ + 8YSZ 25/75 and (d) 8YSZ.

linear intercept length, L, can be calculated by the following formula:

$$L = \frac{1}{N_L}, \tag{2}$$

where N_L is the number of counted grains that fall on a test line laid on the image divided by the length of the test line. From the linear intercept method the grain size, G, is given by [22]:

$$G = 1.570L. \tag{3}$$

The grain size of each sample obtained by the mean linear intercept method is represented in Table 2. It is noted that the grain size of the composite samples decreases from the grain size of the pure 8YSZ with increasing 3YSZ content. The grain size has two opposite effects on the grain boundary resistivity. Smaller grain size is claimed to result in narrower grain boundaries. There are indications that narrower grain boundaries result in higher ionic conductivity [23]. On the other hand, larger grains result in fewer grain boundaries hence reducing

Table 2
Grain size of the pellet samples.

Sample	3YSZ	3YSZ + 8YSZ 75/25	3YSZ + 8YSZ 25/75	8YSZ
Grain size (μm)	2.07	2.72	3.41	4.16

Table 3
Crystallographic data and results of Rietveld refinements performed on X-ray patterns.

Sample	Phase content (%)			Lattice parameters (nm)					Crystallite size (nm)		
	Monoclinic $P2_1/c$ (M)	Tetragonal $P4_2/nmc$ (T)	Cubic Fm3m (C)	Monoclinic $P2_1/c$ (M) a	(T) c	Tetragonal $P4_2/nmc$ (C) a	c	Cubic Fm3m	M	T	C
3YSZ	50	15	35	5.155	5.316	5.157	5.288	5.137	39.4	28.3	26.9
3YSZ + 8YSZ 75/25	36	53	11	5.149	5.287	5.097	5.184	5.135	50.5	32.6	65.6
3YSZ + 8YSZ 25/75	–	–	100	–	–	–	–	5.128	–	–	983
8YSZ	–	–	100	–	–	–	–	5.121	–	–	1300

the grain boundary resistivity. In this study, the composite sample (75% of 8YSZ) with the larger grain size exhibited higher grain boundary conductivity. It can be speculated if there is an intermediate grain size for which the grain boundary resistivity is maximal. In addition, the ''composite effect'' is suggested to give rise to an enhancement in the grain boundary conductivity [8].

3.4. X-ray analysis

X-ray diffraction patterns (see Fig. 12) revealed the presence of three different ZrO_2 structures type for the samples with a high content of 3YSZ. By increasing the 8YSZ content, the pellets crystallinity switch from a majority of monoclinic structure (3YSZ) to a cubic single-phase structure (3YSZ + 8YSZ ratio 25:75 respectively 8YSZ). In the intermediate state 3YSZ + 8YSZ ratio 75:25 the tetragonal phase is predominant. The crystallite sizes of the samples increase by increasing the 8YSZ amount achieving micrometric values for the 8YSZ compound. A minor shift of the diffraction peaks, as well as the powder profile refinements, show that the unit-cell parameters evolve continuously with increasing the 8YSZ content. All the crystallographic data are presented in Table 3.

The increase of the particles size to values in the micrometric range, for the high 8YSZ content, is mainly due

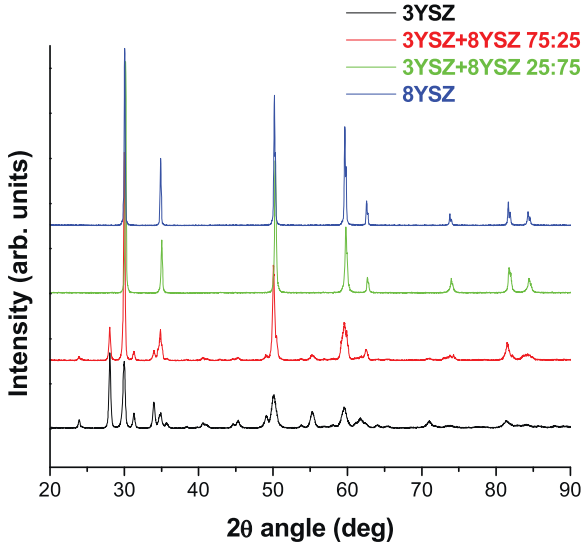

Fig. 12. X-ray diffraction patterns.

the presence of single-phase cubic structure for these compounds. In these cubic single-phase compounds, the significant increase in the particles size is due to the high value of the sintering temperature. The grain boundary effects on the electrical properties in the micrometric particles size of high 8YSZ content compounds is reduced by the nanometric size of the low 8YSZ content compounds.

In the self-supported electrolyte configuration both high conductivity and mechanical strength are required from the ionic conductor. Fulfilling these requirements means to compromise by adding strength to the material at the expense of the conductivity. The combined results from the impedance measurements and the X-ray analysis suggest that the high conductivity of samples with high 8YSZ content can be associated with the cubic structure [1,2]. Since the poor mechanical properties of the pure cubic structure are well known [2,4,7,8] the results indicate that further addition of 3YSZ giving rise to the tetragonal phase is needed in order to improve the mechanical properties of the composite mixture. Therefore further work will be done to optimize the mass ratio between the commercial 3YSZ and 8YSZ in the tape casting slurry to obtain optimal mechanical and electrical properties. Since the mechanical characteristics of the obtained samples were not addressed in the present study further work will also include characterization of the mechanical properties of the composite tapes.

4. Conclusions

In this study water-based tape casting was used to prepare composite 3YSZ/8YSZ electrolytes for SOFC applications. Water-based tape casting was chosen due to health and environmental issues. A commercial acrylic polymer binder, which also functions as dispersant, was used. Crack-free green tapes were obtained by using a carrier speed of 575 mm/min at an under bed heating temperature of 50 °C. The sintering program with a final target temperature 1450 °C and a slow heating rate in the early stage of sintering resulted in fully densified tapes. The XRD analysis showed a cubic single phase structure for the pure 8YSZ and the 3YSZ + 8YSZ composite sample with 75% of 8YSZ. The pure 3YSZ and the 3YSZ + 8YSZ composite sample with 75% of 3YSZ showed the presence of three phases with predominant monoclinic and tetragonal phase, respectively. The impedance measurements performed on the composite samples showed that the

ionic conductivity was modified with respect to the pure materials. High conductivity at higher temperatures was related to the cubic structure. High conductivity at lower temperatures was associated with the reduction of the grain boundary resistance.

Acknowledgments

The authors wish to acknowledge the NFR (Norwegian Research Council) for funding this project. In addition, the authors like to thank Professor Alex C. Hoffmann (Institution of Physics and Technology, University of Bergen) for helpful discussions on the results. Also, the authors are grateful to Senior Engineer Egil Erichsen and Senior Research Engineer Irene Heggstad (The Electron Microscopy Laboratory, University of Bergen) for help using the SEM.

References

[1] S.C. Singhal, K. Kendall, High Temperature Solid Oxide Fuel Cells: Fundamentals, Design and Applications, first edition, Elsevier Ltd., 2003.
[2] S.P.S. Badwal, Zirconia-based solid electrolytes – microstructure, stability and ionic-conductivity, Solid State Ionics 52 (1992), 23.
[3] Y. Arachi, H. Sakai, O. Yamamoto, Y. Takeda, N. Imanishai, Electrical conductivity of the ZrO2–Ln(2)O(3) (Ln = lanthanides) system, Solid State Ionics 121 (1999) 133–139.
[4] A.J. Feighery, J.T.S. Irvine, Effect of alumina addition upon electrical properties of 8 mol.% yttria-stabilised zirconia, Solid State Ionics 121 (1999) 209.
[5] J. Kondoh, H. Shiota, K. Kawachi, T. Nakatani, Yttria concentration dependence of tensile strength in yttria-stabilized zirconia, Journal of Alloys and Compounds 365 (2004) 253–258.
[6] J. Malzbender, R.W. Steinbrech, Fracture test of thin sheet electrolytes for solid oxide fuel cells, Journal of the European Ceramic Society 27 (2007) 2597–2603.
[7] P. Timakul, S. Jinawath, P. Aungkavattana, Fabrication of electrolyte materials for solid oxide fuel cells by tape-casting, Ceramics International 34 (2008) 867–871.
[8] M. Ghatee, M.H. Shariat, J.T.S. Irvine, Investigation of electrical and mechanical properties of 3YSZ/8YSZ composite electrolytes, Solid State Ionics 180 (2009) 57–62.
[9] R.E. Mistler, E.R. Twiname, Tape Casting – Theory and Practice, first edition, The American Ceramic Society, Ohio, US, 2000.
[10] N. Hashimoto, S. Niijima, J.-I. Inagaki, Fabrication of 80 mm diameter-sized solid oxide fuel cells using a water-based NiO-YSZ slurry, Journal of the European Ceramic Society 29 (2009) 3039–3043.
[11] M. Cologna, A.R. Contino, D. Montinaro, V.M. Sglavo, Effect of Al and Ce doping on the deformation upon sintering in sequential tape cast layers for solid oxide fuel cells, Journal of Power Sources 193 (2009) 80–85.
[12] Y.-P. Fu, Y.-C. Liu, S.-H. Hu, Aqueous tape casting and crystallization behavior of gadolinium-doped ceria, Ceramics International 35 (2009) 3153–3159.
[13] Y.-P. Fu, S.-H. Chen, F.-Y. Tsai, S.-H. Hu, Aqueous tape casting and crystallization kinetics of $Ce_{0.8}La_{0.2}O_{1.9}$ powder, Ceramics International 35 (2009) 609–615.
[14] M.P. Albano, L.B. Garrido, Influence of the aging time of yttria stabilized zirconia slips on the cracking behavior during drying and green properties of cast tapes, Ceramics International 34 (2008) 1279–1284.
[15] F. Snijkers, A. de Wilde, S. Mullens, J. Luyten, Aqueous tape casting of yttria stabilised zirconia using natural product binder, Journal of the European Ceramic Society 24 (2004) 1107–1110.
[16] L.F.G. Setz, I. Santacruz, M.T. Colomer, S.R.H. Mello-Castanho, R. Moreno, Fabrication of Sr- and Co-doped lanthanum chromite interconnectors for SOFC, Materials Research Bulletin 46(7) (2011) 983–986, ISSN 0025-5408, doi:10.1016/j.materresbull.2011.03.019.
[17] T. Corporation, Tosoh Advanced Ceramics: Zirconia Powders Basic Grades, http://www.tosoh.com/Products/basic2_grades.htm, 2011.
[18] J. Rodriguez-Carvajal, Recent advances in magnetic-structure determination by neutron powder diffraction, Physica B 192 (1993) 55–69.
[19] T.A. Ring, Fundamentals of Ceramic Powder Processing and Synthesis, first edition, Academic Press, 1996.
[20] H. Tikkanen, C. Suciu, I. Waernhus, A.C. Hoffmann, Dip-coating of 8YSZ nanopowder for SOFC applications, Ceramics International 37 (2011) 2869–2877.
[21] E. Barsoukov, J.R. MacDonald (Eds.), Impedance Spectroscopy Theory, Experiment and Applications, second edition, Wiley, 2005.
[22] M.I. Mendelson, Average grain size in polycrystalline ceramics, Journal of the American Ceramic Society 52 (1969).
[23] M.F. Han, X.L. Tang, H.Y. Yin, S.P. Peng, Fabrication, microstructure and properties of a YSZ electrolyte for SOFC, Journal of Power Sources 165 (2007) 757–763.